

# GETAM: Gradient-weighted Element-wise Transformer Attention Map for Weakly-supervised Semantic segmentation

Weixuan Sun<sup>1</sup>, Jing Zhang<sup>1</sup>, Zheyuan Liu<sup>1</sup>, Yiran Zhong<sup>2</sup>, Nick Barnes<sup>1</sup>  
Australian National University<sup>1</sup> SenseTime<sup>2</sup>

## Abstract

Weakly-supervised semantic segmentation (WSSS) is challenging, particularly when image-level labels are used to supervise pixel-level prediction. To bridge their gap, a Class Activation Map (CAM) is usually generated to provide pixel-level pseudo labels. CAMs in Convolutional Neural Networks suffer from partial activation i.e. only the most discriminative regions are activated. Transformer-based methods, on the other hand, are highly effective at exploring global context, potentially alleviating the “partial activation” issue. In this paper, we propose the first transformer-based WSSS approach, and introduce the Gradient-weighted Element-wise Transformer Attention Map (GETAM). GETAM shows fine scale activation for all feature map elements, revealing different parts of the object across transformer layers. Further, we propose an activation-aware label-completion module to generate high-quality pseudo labels. Finally, we incorporate our methods into an end-to-end framework for WSSS using double-backward propagation. Extensive experiments on PASCAL VOC and COCO dataset demonstrate that our results outperform not only the state-of-the-art end-to-end approaches by a significant margin, but also most of the multi-stage methods.

## 1. Introduction

Recent work on 2D image semantic segmentation has achieved great progress via deep fully convolutional neural networks (FCNs) [43]. The success of these models [13–15, 77] comes from large training datasets with pixel-wise labels, which are laborious and expensive to obtain. To relieve the labeling burden, multiple types of weak labels have been explored, including image-level labels [2, 21, 28], points [6], scribbles [39, 58, 61] and bounding boxes [16, 36, 46, 47]. In this paper, we focus on weakly-supervised semantic segmentation (WSSS) with image-level labels.

To bridge the gap between pixel-level classification and

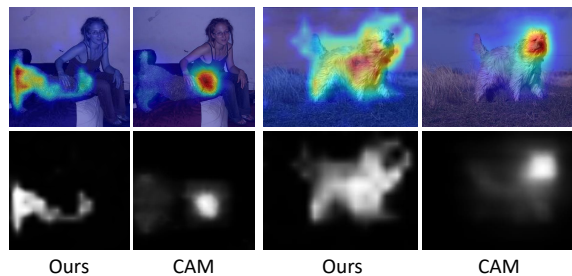


Figure 1. Comparison between CAM and our GETAM. Baseline CAMs (“CAM”) focus too much on discriminative regions and are over smoothed. Our GETAM generates class-wise attention maps (“Ours”), capturing better object shapes.

image-level annotation, it is essential to localize object classes in the image from image-level labels. Most WSSS methods rely on the Class Activation Map (CAM) [78] as initial seeds from the image-level label to learn pixel-level labeling. Typical multi-stage image-level WSSS methods usually adopt progressive steps [8, 23, 31, 65, 70, 72, 75]: 1) training a CNN classifier to obtain object activation maps [8, 23, 26, 31, 65, 78]; 2) refining the maps with non-learning [69] or learning based methods [2, 28] to obtain pseudo labels; and 3) using these pseudo labels for fully-supervised training of an off-the-shelf semantic segmentation network, such as Deeplab [14]. Alternatively, recently end-to-end WSSS methods have become more prevalent [3, 72]. In both cases, the quality of the initial response map plays a key role in WSSS. However, it is recognized by many approaches [8, 23, 31, 57, 65, 67, 69, 70, 72, 75] that CAMs suffer from two issues: 1) CAMs tend to only activate the discriminative regions of objects; 2) the rough object activation of CAMs loses accurate object shapes. The main causes of above issues are limited receptive fields and the progressively down-sampled CNN feature maps.

Transformers [60] have shown great success in various computer vision tasks, but transformer-based WSSS is yet to be well studied. We argue that transformers have several appealing mechanisms for WSSS. First, transformers are

highly effective at exploring global context with long-range dependency modelling. Hence, one would expect they could address issues regarding the limited visual field of CNNs. Also, after computing the initial embedding, vision transformers have a constant global receptive field at every layer with constant dimensionality, which could retain more accurate structure information [45, 49]. Further, transformers use self-attention to spread activation across the *entire* feature map rather than just discriminative regions, leading to more uniform activation. We show that these properties are beneficial for generating object activation maps, as well for other dense prediction tasks [5, 42, 49, 62].

Unfortunately, we observe extensive noise if we simply transplant the conventional CAM [78] to vision transformers (Fig. 2). Such noise leads to poor performance and is believed to arise along with the global context ability of the transformer architecture [76]. To address this, we closely study activation and propagation of the feature maps through transformer layers. Particularly, we explore element-wise weighting to couple the attention map (*i.e.*  $Q \times K$ ) with its squared gradient to place greater emphasis on the gradient. Further, as attention is progressively propagated and refined through the transformer layers, it reveals different parts of the object. We sum the attention maps through transformer layers, leading to more uniformly activated object maps, as shown in Fig. 1. We refer to this as the **Gradient-weighted Element-wise Transformer Attention Map (GETAM)**.

After obtaining class-wise attention maps, we propose **activation aware label completion**, combining the obtained object activation with off-the-shelf saliency maps to generate pseudo segmentation labels. In this way, we refine foreground object masks and actively discover objects in the background, leading to high-quality pseudo labels.

Finally, we propose a **double-backward propagation** mechanism to implement our framework in an end-to-end manner. Most WSSS methods require multiple stages, involving multiple models with different pipelines and tweaks, making them hard to train and implement. Although the existing end-to-end approaches [3, 47, 48, 71, 72] are elegant, they show substantially inferior performance to multi-stage methods. Our method is easy to implement and extensive experiments on the PASCAL VOC [18] and COCO [41] datasets verify its effectiveness.

Our contributions can be summarised as: 1) We introduce the first weakly-supervised semantic segmentation framework based on vision transformer networks. The key to its performance is the Gradient-weighted Element-wise Transformer Attention Map (GETAM), capturing better object shapes than traditional CAMs. 2) We present activation-aware label completion guided by saliency maps to generate high-quality pseudo labels. 3) We propose a double-backward propagation mechanism to implement our

method in an end-to-end manner. Despite its simplicity, our method greatly boosts the performance of single-stage WSSS, and it is the first one to be competitive with multi-stage methods.

## 2. Related Work

### 2.1. Weakly Supervised Semantic Segmentation

To save labeling cost, many WSSS methods have been proposed, including those using image-level labels [2, 8, 37, 47, 65, 70, 72], scribbles [39], points [6], and bounding boxes [16, 36, 46, 56]. We mainly focus on image-level models, which can be grouped into two families: multi-step, and one-step end-to-end methods.

**Multi-step methods** [2, 7, 8, 23, 31, 37, 65, 70, 72, 75] refine one or multiple sub-modules within the multi-model framework. Among them, [2] proposes to predict semantic affinity between a pair of adjacent image coordinates supervised by initial activation, the network is then used to guide a random walk to generate pseudo labels. [7, 23] utilize Mixup data augmentation to calibrate uncertainty in prediction. They randomly mix an image pair and feed into the network, which forces the model to pay attention to other regions in the image. [37] directly uses saliency maps to constrain object activation during classification training, so the CAMs can better follow object shapes.

**One-step methods** [47] adopts an expectation-maximisation mechanism, where intermediate predictions are used as segmentation labels. [72] presents an end-to-end framework to train classification and segmentation simultaneously, and integrates a method to obtain reliable segmentation pseudo labels. [3] introduces normalised Global Weighted Pooling (nGWP) to obtain better CAMs for segmentation, and adopts a Stochastic gate to encourage information sharing between deep features and shallow representations to deal with complex scenes. With all above solutions, end-to-end WSSS is still far from being well-studied, and has clear performance gaps from multi-step methods.

### 2.2. Network Visualization

Various works have been proposed for network visualization and are leveraged for tasks like weak semantic segmentation and weak object localization. CAM [78] replaces the first fully-connected layer in image classifiers with a global average pooling layer to calculate class activation map. Grad-CAM family methods [9, 30, 52] flow the class-specific gradients to each feature map and adopt different ways to obtain a weighted sum of feature maps for visualization. For the vision transformer, [22] proposes to couple semantic-agnostic attention maps and semantic aware maps for weakly supervised object localization. [10, 11] employ LRP-based relevance [4] combined with gradients to ex-

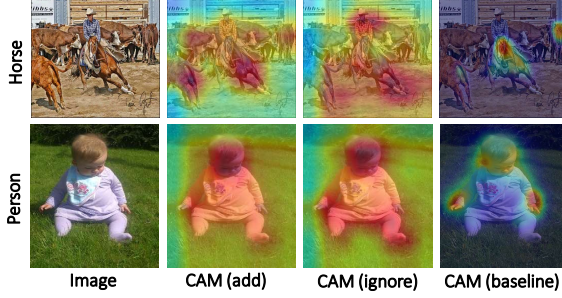


Figure 2. Comparison between CAMs generated by ViT and CNN. We explore different strategies to manipulate the output feature map  $O_{CLS} \in \mathbb{R}^{1 \times d}$  from the transformer to generate final feature maps. **add**: we directly add  $O_{CLS} \in \mathbb{R}^{1 \times d}$  to every location of  $O[1:] \in \mathbb{R}^{n \times d}$ . **ignore**: we ignore  $O_{CLS} \in \mathbb{R}^{1 \times d}$ , and simply feed  $O[1:]$  into GAP. **baseline**: CNN CAM (ResNet38).

plore the interpretability of transformer attention. However, none of above methods are specially designed for WSSS.

### 3. Revisiting CAM in ViT

In this section, we revisit conventional CAMs [2] used in most WSSS methods. We present a pilot experiment to investigate different activation mechanisms in convolutional and transformer backbones, demonstrating that the conventional CAM [78] and Grad-CAM [51] methods used in existing WSSS methods *cannot* be trivially transplanted to transformer-based approaches.

To generate a CAM [78] in a CNN classifier, [78] feeds convolutional feature maps  $f$  into global average pooling (GAP) followed by a fully-connected layer to produce a categorical output. For an image  $I$ , activation maps for category  $c$  are defined as:  $A^c(x, y) = \theta_p^c f(I(x, y))$ , where  $\theta_p^c$  is classifier’s weight of class  $c$  and  $f(I(x, y))$  is the extracted feature at location  $(x, y)$ . Then, we copy the same CAM structure to the transformer backbone. Given the extracted feature maps  $O \in \mathbb{R}^{(n+1) \times d}$  from the transformer network, we obtain  $O[1:] \in \mathbb{R}^{n \times d}$ , where  $n = h \times w$  is the input image patch size, and  $d$  is the latent feature embedding dimension. The first row  $O_{CLS} \in \mathbb{R}^{1 \times d}$  is the [class] token. We explore different strategies to manipulate  $O_{CLS}$  and generate a feature map  $O \in \mathbb{R}^{h \times w \times d}$ . We then use global average pooling (GAP) and a fully-connected layer as the classifier to make predictions and obtain CAMs.

As shown in Fig. 2, if we simply follow the conventional method, the generated CAMs are flawed. Due to the self-attention mechanism, every feature map location encodes information from the entire image in a fully connected manner. However, classification loss is indifferent to extensive activation across objects, requiring only a sufficient pooled global average. So per-location features may not contribute to local classification predictions, and activation shows noise across the image, or can be completely wrong. Reliable CAMs are crucial for end-to-end WSSS,

but CNN-based CAMs cannot be naively migrated to vision transformers, *i.e.* changing backbones of current end-to-end WSSS methods to transformer architectures is non-trivial.

## 4. Approach

We show the overview of our framework in Fig. 3. First of all, we introduce GETAM (Gradient-weighted Element-wise Transformer Attention Map), which generates better class-wise attention maps with image-level labels. Then, we introduce activation aware label completion, which uses saliency information to produce high-quality pseudo segmentation labels from the activation maps. Finally, we present double-backward propagation to implement our method into a single-stage framework.

### 4.1. GETAM

As discussed in Sec. 3, conventional CAM generation methods used in CNN backbones fail to generate reliable CAMs in transformers. Thus, inspired by Grad-CAM [51], we design a gradient-based method to obtain class-wise attention maps for vision transformer networks. Note that our method is substantially different to Grad-CAM [51], albeit also based on gradients. In Grad-CAM [51], classification predictions are back propagated to the output feature maps of the final convolutional layer. The obtained gradients are global average pooled, and used to weigh neuron importance of those feature maps.

However, transformer networks use different structures for predictions. A transformer network consists of several successive transformer blocks, each composed of multi-head self-attention modules and feed-forward connections. The  $i^{th}$  self-attention module on one of the multiple heads in a transformer block is defined as:

$$\text{Attention}(Q^i, K^i, V^i) = \text{softmax}\left(\frac{Q^i K^{iT}}{\sqrt{d}}\right) V^i = A^i V^i, \quad (1)$$

where  $Q^i, K^i, V^i$  are query, key and value matrices  $\in \mathbb{R}^{(n+1) \times d}$ ,  $n$  is number of patches ( $n = w \times h$ ) and  $d$  is feature dimensions. The [class] is an extra learnable token in the first row of these matrices [17]. As shown in Fig. 5,  $A^i \in \mathbb{R}^{n \times n}$  is the attention matrix which encodes the attention coefficient between any two positions in input images, *i.e.*, every image token has contextual information from all other tokens. Consequently, the [class] token attends to all token information across the image. However, it is not affected by itself as it does not represent an image location. We define  $A^i[0, 1:] = A_{CLS}^i \in \mathbb{R}^n$ . We can reshape  $A_{CLS}^i \in \mathbb{R}^n$  back to the shape of the image  $A_{CLS} \in \mathbb{R}^{h \times w}$ , and obtain a class-agnostic attention map, where every position in the map denotes its contribution to classification. In every transformer block with multiple self-attention heads, we define  $A_{CLS}^i$  as the average across all heads for simplicity. As empirically verified in [22], it aggregates attention from all self-attention heads to display

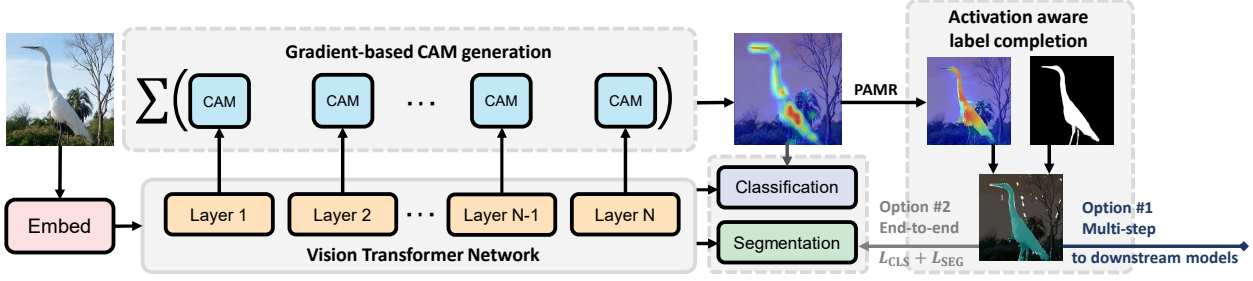


Figure 3. Overview of the proposed end-to-end WSSS framework. We back-propagate classification predictions, and compute the sum of class-wise attention maps from cascaded transformer blocks. Then we generate high-quality pixel-wise pseudo labels guided by saliency maps. The pseudo segmentation labels are used to supervise the segmentation branch of our vision transformer in an end-to-end manner, or train a separate semantic segmentation network.

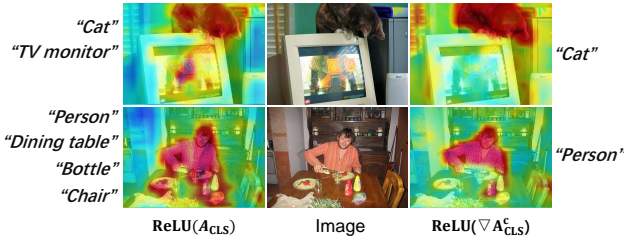


Figure 4. Visualizations of class-agnostic attention maps (column 1) and class-wise gradient maps (column 3). Class-agnostic attention maps show the regions that possibly contribute to the classification predictions. Class-wise gradient maps display class specific regions and retain clear object shapes.

the object extent that possibly contributes to classification predictions (see the first column of Fig 4).

As  $A_{CLS}^i$  is class agnostic, we couple it with its gradients  $\nabla A^i$  to obtain the class-wise attention map. We back-propagate the classification score  $y^c$  for each class  $c$ . The graph is differentiated using the chain rule through the transformer network. In the  $i^{th}$  block, the gradient map  $\nabla A^{i,c}$  is obtained with respect to the attention matrix  $A^i$ . Referring to Fig. 5, we extract the corresponding gradient map  $\nabla A_{CLS}^{i,c} \in \mathbb{R}^n$  of  $A_{CLS}^i$  with respect to class  $c$ . As discussed in [9, 30, 51], a positive gradient corresponding to a location in the feature map indicates that it has a positive influence on the prediction score of the target class. We find that this assertion still holds in vision transformers. Each position in  $\nabla A_{CLS}^{i,c}$  indicates the contribution of this token to the classification output of class  $c$ .

**Attention Gradient Coupling.** We observe that  $A_{CLS}^i$  shows class-agnostic areas with possibly targeted objects and relatively clean background. Further, we find  $\nabla A_{CLS}^{i,c}$  is noisy but retains clear object shapes(see column 3 of Fig 4). Based on the above observations, we propose to combine the attention map and its gradient inside every transformer block to generate reliable class-wise attention as shown in Fig. 5. Formally, the class-wise attention map of block  $i$  for

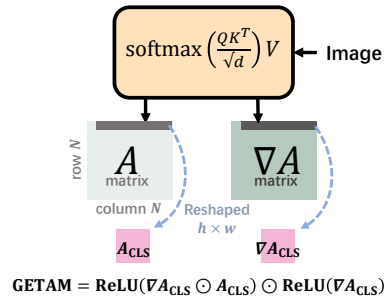


Figure 5. GETAM generation in a single transformer block.  $A_{CLS}^i$ : class-agnostic attention map.  $\nabla A_{CLS}$ : class-wise gradient map.

class  $c$  is defined as:

$$\text{GETAM}_c^i = \text{ReLU} \left( \nabla A_{CLS}^{i,c} \odot A_{CLS}^i \right) \odot \text{ReLU}(\nabla A_{CLS}^{i,c}) \quad (2)$$

We first use an element-wise multiplication  $\odot$  to couple the attention map  $A_{CLS}^i$  with its gradient map  $\nabla A_{CLS}^{i,c}$ . Then, we perform another element-wise multiplication with  $\text{ReLU}(\nabla A_{CLS}^{i,c})$ . Different from GradCAMs which uses the Global Average Pool of the Gradients, our attention map is weighted element-wise by the square of the gradient, and negative responses of attention and gradients are eliminated by the ReLUs. Our Attention-Gradient coupling can better harvest spatial locations that have positive contributions to the targeted class, while suppressing noisy regions.

**Successive Attention Aggregation.** After obtaining the class-wise attention map in a single transformer block, here we present an analysis on how to aggregate class attention maps from cascaded transformer blocks.

As commonly recognized by existing WSSS methods [55, 55, 57, 65, 74], the attention maps should not respond too sparsely (*i.e.*, only highlighting discriminative regions), nor be overly smoothed. Based on the above requirements, we first visualize the class-wise attention maps from different transformer blocks in Fig. 6. Unlike CNNs where low-level features contain too much noise that buries useful information [30, 66], we observe that the cascaded maps in vision transformers tend to focus on discriminative regions.



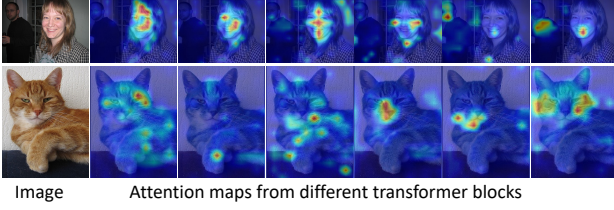


Figure 6. Sample images of the attention maps from different transformer blocks. The cascaded maps focus on different object regions without low-level noise. In the first row, the network focuses on different people in the foreground and background separately at different layers. Recommend viewing digitally.

For instance, in Fig. 6 (bottom), attention maps from different layers reveal different regions of the cat (*e.g.*, cheek, nose, chin, body and hand). Thus, it is crucial to choose an appropriate fusion method to combine different class-wise attentions maps.

In this view, we present a numerical analysis of different fusion approaches (Fig. 7). On the PASCAL VOC [18] training set, we apply three commonly adopted operations (element-wise multiplication, summation and matrix multiplication) to fuse the successive maps, and then we visualize the distributions of the fused results after normalization. As illustrated in Fig. 7, element-wise multiplication will concentrate the values and most areas are suppressed, which is because the activation is canceled if the value is low in any level of the transformer. Contrarily, matrix multiplication (dot production) will smooth the attention, leading to additional noise in non-object regions. Based on the above analysis, we propose summation aggregation across cascaded attention maps, which encourages the final class-wise attention maps to cover accurate object areas and does not over-smooth them.

Formally, the attention maps are added through  $L$  layers of the vision transformer:

$$\text{GETAM}_c = \sum_i^L (\text{GETAM}_c^i) \quad (3)$$

Eq. 3 shows that GETAM from the cascaded blocks captures reliable object shapes and suppress the noise. Qualitative comparison is shown in the supplementary material.

## 4.2. Activation Aware Label Completion

GETAM generates reliable class-wise attention maps using classification predictions. However, the attention maps cannot be directly used as pseudo labels for semantic segmentation training since it is gray-scale, so it requires refinements. To achieve this, we first adopt pixel adaptive mask refinement (PAMR) [3], a parameter-free recurrent module that efficiently refines pixel labels using local information. Then, we propose *saliency constrained object*

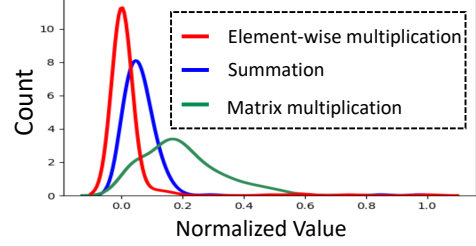


Figure 7. Distributions of class-wise attention maps using different fusion methods. Element-wise multiplication concentrates the distribution, but suppresses most areas. Matrix multiplication (dot production) smooths the attention, leading to additional noises.

*masking* and *high activation object mining* to obtain high-quality pseudo labels. The two solutions work collaboratively to supports accurate segmentation of salient objects, but does not suppress non-salient objects. This leads to improved performance in multiple and single object images.

**Saliency Constrained Object Masking.** We observe that due to the global context of self-attention, candidate regions that may contribute to classification are activated, leading to high recall of our activation maps for targeted objects. Saliency maps from off-the-shelf models can provide precise foreground object shapes and have been used as background cues to many WSSS approaches [19, 29, 34, 37, 54, 64, 69]. We leverage the saliency mask to constrain activated object regions, which is particularly necessary in our case for GETAM to combat additional activation on object boundaries.

First, based on object activation maps  $M_{fg} = \text{GETAM} \in \mathbb{R}^{C \times h \times w}$  which have  $C$  foreground classes, we calculate an arbitrary background channel in a similar way to [2]:  $M_{bg} = \left[ 1 - \max_{c \in C_{fg}} (M_{fg}^c(i)) \right]^\gamma$ , where  $\gamma > 1$  is a parameter to adjust background labels and  $i$  is the pixel position. Then we concatenate  $M_{bg}$  onto  $M_{fg}$  to form activation maps  $M$ , and use  $\text{argmax}(M)$  to find the per-pixel highest activation. After that, we can locate all possible objects in both salient and non-salient regions with rough boundaries, as shown in Fig. 8(a). Then we adopt saliency maps to refine object boundaries of  $M$ , where the current temporary background (0) is set to unknown (255) and all non-salient regions in the saliency map are set to background (0). This is based on the observation that the saliency maps normally provide accurate object boundaries [37, 63, 69]. In other words, with saliency constrained object masking, we extract reliable foreground object labels and set low-activated object regions to unknown (255), and set non-salient regions to be background (0). Formally, consider activation maps  $M$  with saliency map  $S$ , pixel  $i$  of our pseudo label  $P_{seg}$  is:

$$P_{seg}(i) = \begin{cases} c & \text{argmax}(M) = c, S(i) = 1 \\ 255 & \text{argmax}(M) = 0, S(i) = 1 \\ 0 & S(i) = 0 \end{cases} \quad (4)$$

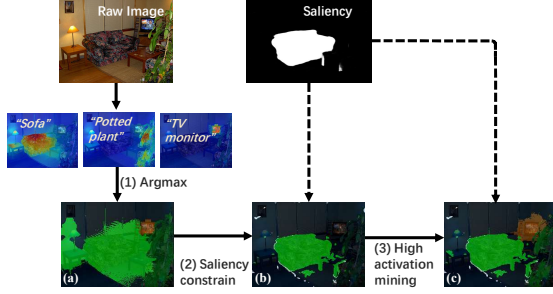


Figure 8. An example of activation aware label completion module processing. (a) First locate all objects with activation maps. (b) With the saliency constraint, we obtain accurate shape for salient objects, however, non-salient objects are suppressed. (c) High activation mining correctly locates suppressed background objects. Enlarge the figure by 3 times for best viewing.

**High Activation Object Mining.** With “saliency constrained object masking”, we obtain  $P_{seg}$ , where the structure of the instances that are consistent with salient objects is refined. However, recall that existing salient object detection models are trained with class-agnostic objects and center bias, and so non-salient objects may masked as background. As shown in Fig. 8(b), the TV monitor and potted plant are mislabeled as background. We then propose a high activation object mining strategy to solve this issue.

GETAM can correctly locate all desired objects in both salient and non-salient regions as shown in Fig. 8(a). For class  $c$ , we find high confident regions by searching for pixels with activation greater than a threshold  $\alpha$  in non-salient regions. We treat these as pseudo labels of class  $c$  in the background (see Fig. 8 (c)). In addition, we maintain another high-confidence conflict mask  $M_{conflict}$  to register conflict areas in non-salient regions. That is, if a pixel is highly activated by more than one class in the background, we regard it as conflict and label it as unknown (255) to avoid introducing incorrect labels. Formally, high activation object mining is defined:

$$P_{seg}(i) = \begin{cases} c & M(i) > \alpha, M_{conflict}(i) = 1, S(i) = 0 \\ 255 & M(i) > \alpha, M_{conflict}(i) > 1, S(i) = 0 \\ 0 & M(i) < \alpha, S(i) = 0 \end{cases} \quad (5)$$

where  $\alpha$  is the high confidence threshold, empirically set to 0.9, *i.e.*, if the activation at a pixel of class  $c$  is higher than 90% of all activation of the same object class, we regard it as highly activated and label it as  $c$ , otherwise as background (0). We ablate  $\alpha$  in detail in the supplementary material.

We give a quantitative comparison of our generated pseudo labels to other methods in Table 1. Our high-quality pseudo labels can be directly used to supervise an off-the-shelf semantic segmentation model. They can also supervise a segmentation branch of the same vision transformer

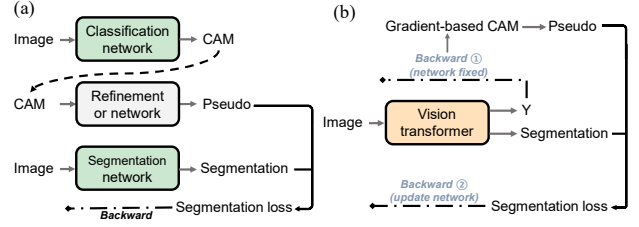


Figure 9. WSSS framework conceptual comparison: (a) Multi-step methods, which involve multiple stages and networks; (b) Proposed transformer approach, can be trained in one go.

backbone in an end-to-end manner. We will introduce in the next section.

### 4.3. Single-stage Double-backward Propagation

Most current WSSS methods [8, 23, 31, 65, 70, 72, 75] require multiple steps, which usually involve training multiple models with different pipelines and tweaks. Inter-dependencies between the steps can easily influence final performance. Further, the vision transformer shows properties that are especially advantageous for dense prediction tasks like semantic segmentation [5, 42, 49, 62].

Based on above considerations, we propose an unified framework to train our WSSS method in an end-to-end manner. As shown in Fig. 3, the framework has two parallel branches, *i.e.* a classification and a semantic segmentation branch. Both branches share the same vision transformer backbone, and update the entire network simultaneously during training.

As illustrated in Fig. 9, the core of our approach is double-backward propagation. That is, the network back propagates to compute GETAM without updating the network to obtain pseudo labels, then back propagates again to optimize the network supervised by these pseudo labels. Each iteration consists of two back propagation operations but the network is only updated once. Specifically, we first perform a forward pass to produce classification predictions  $Y$ , while without calculating the classification loss. Then, for the target class  $c$ , we back propagate its output  $y^c$  to obtain GETAM. We iterate to obtain class-wise attention maps for every class appearing in the image, and use them to generate pseudo segmentation labels. In the second back propagation step, we clear the gradients and perform another forward pass to generate classification and semantic segmentation predictions. With the pixel level pseudo labels and image level labels, we train our network with classification prediction and semantic prediction from the second back propagation. Back propagating GETAM leads to better localization of objects and segmentation performance. The proposed double-backward propagation does not rely on multi-step WSSS training, and shows competitive performance (see Table 4).

| Methods                     | Train       | Val         |
|-----------------------------|-------------|-------------|
| <i>Multi stage methods</i>  |             |             |
| CAM + RW + CRF [2]          | 59.7        | —           |
| CAM + RW + IRN [1]          | 66.5        | —           |
| SEAM [64] + RW + CRF        | 63.6        | —           |
| SC-CAM [8] + RW + CRF       | 63.4        | 61.2        |
| EDAM [67] + CRF             | 68.1        | —           |
| AdvCAM [35] + RW + CRF      | 68.0        | —           |
| AdvCAM [35] + IRN + CRF     | 69.9        | —           |
| <i>Single stage methods</i> |             |             |
| 1-stage-wseg [3]            | 64.7        | 63.4        |
| 1-stage-wseg [3] + CRF      | 66.9        | 65.3        |
| <b>Ours</b>                 | <b>69.6</b> | <b>66.7</b> |

Table 1. Pseudo label mIoU on PASCAL VOC *train* and *val* set. Our results (bold) are obtained on ViT-Hybrid [17].

## 5. Experiments

### 5.1. Setup and Implementation Details

Our method is evaluated on the PASCAL VOC [18] and MS-COCO datasets [41]. PASCAL VOC [18] has one background and 20 foreground classes. The official dataset consists of 1,446 training images, 1,449 validation and 1456 test images. We follow common practice [24], augmenting the training set to form a total of 10,582 images. MS-COCO 2014 [41] contains 81 classes including the background class with 80k train and 40k val images, which is more difficult for WSSS. In addition, we adopt [45] as our saliency detection model by re-implementing it to generate saliency maps on both datasets. The backbone network of our end-to-end framework is ViT [17] with 12 cascaded transformer blocks. We also test our method on other backbones including ViT-Hybrid [17], DeiT [59] and DeiT-Distilled [59] with 12 transformer blocks.

For multi-stage training, we use the generated pseudo labels to train Deeplab v2 [14] with the ResNet-101 backbone. For our end-to-end framework, classification and segmentation branches share the same vision transformer backbone. For the segmentation branch, we adopt the decoder from [49]. We train our network for 50 epochs, separated into two stages. In the first 25 epochs we train our network only using the classification loss  $L_{cls}$  in order to generate reliable class attention maps. In the remaining 25 epochs we switch on the segmentation branch. In semantic segmentation training, we compute the cross entropy loss  $L_{seg}$  between the segmentation predictions and pseudo labels. Further, as saliency maps are provided, we calculate the binary cross entropy loss  $L_{sal}$  between the predicted background channel and saliency maps to further refine the object shapes. Our final end-to-end training loss is defined as  $L = L_{cls} + L_{seg} + L_{sal}$ . Our model is implemented with PyTorch, with reproduction details in the supplementary material. The codebase will be released upon acceptance.

| Backbone       | MIoU (Val) | MIoU (Test) |
|----------------|------------|-------------|
| ResNet38 [72]  | 62.6       | 62.9        |
| ViT            | 67.9       | 68.8        |
| ViT-Hybrid     | 70.4       | 69.9        |
| DeiT           | 66.0       | 68.9        |
| DeiT-Distilled | 69.7       | 70.8        |

Table 2. Our performances on different vision transformer backbones compared to the CNN-based baseline.

| Model    | Backbone | CAM generation | Pseudo generation | mIoU(val) |
|----------|----------|----------------|-------------------|-----------|
| RRM [72] | CNN      | CAM [78]       | CRF [33]          | 62.6      |
| #1       | CNN      | CAM [78]       | Activation aware  | 64.7      |
| #2       | ViT      | CAM [78]       | Activation aware  | 55.3      |
| #3       | ViT      | GETAM          | Activation aware  | 70.4      |

Table 3. Ablation studies for substituting each part of our method (in bold). RRM [72]: baseline; #3: our fully configured model.

### 5.2. Experiment Analysis

**Pseudo Label Quality.** Pseudo label quality is crucial to semantic segmentation performance for WSSS. We extract the generated pseudo labels in our end-to-end training process and evaluate them for quality with the PASCAL VOC ground-truth. The results in Table 1 show that using GETAM in our double gradient-based method and our activation aware label completion method, the generated pseudo segmentation labels outperform all end-to-end methods. Further, recent state-of-the-art multi-step approaches focus on obtaining pseudo labels using sophisticated pipelines and training multiple networks, and our pseudo labels are still comparable to the best of these. Also, our pseudo labels can be directly used to supervise existing semantic segmentation networks and achieve competitive high-quality multi-step results.

#### Results with Different Vision Transformer Backbones.

We investigate different vision transformer backbones including ViT, ViT-Hybrid [49], DeiT and DeiT-Distilled [59] in our end-to-end WSSS framework. As reported in Table 2, our method performs consistently better than baseline end-to-end WSSS method based on CNN backbones ([72] in particular), validating the effectiveness of our approach. Also, the similar performance of our method with the above two types of backbones illustrates the robustness of our model w.r.t. vision transformer backbones. Note that ViT-Hybrid is pre-trained on JFT-300M dataset [53], while DeiT-Distilled is pre-trained on ImageNet1K. The similar performance and visual results (see Fig. 10) show that our performance gain does not rely on pre-training on JFT-300M.

### 5.3. Source of Improvements (Ablation Studies)

In this section, we conduct multiple experiments to show the effectiveness of different components in our single-stage method. Our baseline is RRM [72], which adopts [78] to obtain baseline CAMs from a CNN backbone, and refines

the CAMs into pseudo labels using CRF. As shown in Table 3, in #1, we replace CRF with our proposed activation aware label completion, which improves result by 2.1% mIoU. Subsequently in #2, we naively change the backbone from CNN to the vision transformers [17] and only get 55.3% mIoU. As discussed in Sec. 3, changing backbone of existing WSSS to transformer is non-trivial. Due to the different activation mechanism, conventional CAM will perform poorly. Finally, in #3, we switch on GETAM and show the performance of our fully configured model. It validates that simple backbone changing is ineffective and GETAM can leverage the power of vision transformer networks.

#### 5.4. Comparison to the State-of-the-art Methods

**PASCAL VOC** In Table 4, we give a detailed comparison of our proposed approach with other WSSS methods. In the Multi-stage section, we compare the segmentation performance of the proposed method with recent multi-stage WSSS approaches, we achieve mIoUs of 70.6% and 70.4% on the val and test sets respectively, which outperform most state-of-the-art methods. In the single-stage section, we achieve significantly improved performance over all existing end-to-end methods. Although previous state-of-the-art method JointSaliency [71] also utilizes saliency and image-level labels, our approach achieves an impressive 7.1% mIoU increase. Second, our proposed approach is the first method that achieves comparable performance to multi-step WSSS methods, which employ sophisticated pipelines and train multiple networks. Despite the fact that NSRM [69] trains multiple networks with many inter-dependencies, it outperforms our ViT-Hybrid result by only 0.3% mIoU on *test* but at the cost of substantial complexity.

**MS-COCO** To further demonstrate the proposed method’s generalization ability, we evaluate it on the challenging MS-COCO dataset [41]. As shown in Table 5, our method achieves 34.9% mIoU, which is superior to previous methods. Notably, our method is the first end-to-end WSSS result reported on MS-COCO [41], which extensively saves the training complexity. And the result shows that our method can effectively generalize to different complex scenes.



Figure 10. Qualitative segmentation results on PASCAL VOC. left: ground truth. Middle: Results from ViT-Hybrid [17]. Right: Results from DeiT-Distilled [59]. More qualitative results are presented in the supplementary material.

|                      | Method                        | Backbone       | Sup.   | val         | test        |
|----------------------|-------------------------------|----------------|--------|-------------|-------------|
| Multi-stage methods  | Affinity [2] (CVPR2018)       | ResNet38       | I      | 61.7        | 63.7        |
|                      | SEAM [65] (CVPR2020)          | ResNet38       | I      | 64.5        | 65.7        |
|                      | BES [12] (ECCV2020)           | ResNet101      | I      | 65.7        | 66.6        |
|                      | SC-CAM [8] (CVPR2020)         | ResNet101      | I      | 66.1        | 65.9        |
|                      | CONTA [73] (NeurIPS2020)      | ResNet38       | I      | 66.1        | 66.7        |
|                      | CDA [55] (ICCV2021)           | ResNet101      | I      | 66.1        | 66.8        |
|                      | MCS [54] (ECCV2020)           | ResNet101      | I+S    | 66.2        | 66.9        |
|                      | ECS-Net [55] (ICCV2021)       | ResNet38       | I+S    | 66.6        | 67.6        |
|                      | EME [20] (ECCV2020)           | ResNet101      | I+S    | 67.2        | 66.7        |
|                      | ICD [19] (CVPR2020)           | ResNet101      | I+S    | 67.8        | 68.0        |
|                      | CPN [74] (ICCV2021)           | ResNet101      | I      | 67.8        | 68.5        |
|                      | AuxSegNet [68] (ICCV2021)     | ResNet101      | I+S    | 69.0        | 68.6        |
|                      | PMM [38] (ICCV2021)           | ResNet101      | I      | 70.0        | 70.5        |
|                      | NSRM [69] (CVPR2021)          | ResNet101      | I+S    | 70.4        | 70.2        |
|                      | Ours                          | ResNet101      | I+S    | <b>70.6</b> | <b>70.4</b> |
| Single-stage methods | EM [47] (ICCV2015)            | VGG16          | I      | 38.2        | 39.6        |
|                      | TransferNet [25] (CVPR2016)   | VGG16          | I+COCO | 52.1        | 51.2        |
|                      | CRF-RNN [50] (CVPR2017)       | VGG16          | I      | 52.8        | 53.7        |
|                      | RRM [72] (AAAI2020)           | ResNet38       | I      | 62.6        | 62.9        |
|                      | 1-stage-wseg [3] (CVPR2020)   | ResNet38       | I      | 62.7        | 64.3        |
|                      | JointSaliency [71] (ICCV2019) | DenseNet169    | I+S    | 63.3        | 64.3        |
|                      | Ours                          | ViT-Hybrid     | I+S    | <b>70.4</b> | <b>69.9</b> |
|                      | Ours                          | DeiT-Distilled | I+S    | <b>69.7</b> | <b>70.8</b> |

Table 4. Comparison with the state-of-the-art methods on PASCAL VOC 2012 *val* and *test* sets. Our results are in bold. Different supervisions are used: I: image-level label. COCO: MS-COCO [41], S: saliency. We categorize WSSS methods into multi-stage methods and single stage methods.

| Method                    | Backbone   | mIoU (val)  |
|---------------------------|------------|-------------|
| SEC [32] (CVPR2016)       | VGG16      | 22.4        |
| DSRG [28] (CVPR2018)      | VGG16      | 26.0        |
| Wang [64] (IJCV2020)      | VGG16      | 27.7        |
| Luo [44] (AAAI2020)       | VGG16      | 29.9        |
| SEAM [65] (CVPR2020)      | ResNet38   | 31.9        |
| CONTA [73] (NeurIPS2020)  | ResNet38   | 32.8        |
| CDA [55] (ICCV2021)       | ResNet50   | 33.7        |
| AuxSegNet [68] (ICCV2021) | ResNet101  | 33.9        |
| Ours                      | ViT-Hybrid | <b>34.9</b> |

Table 5. Comparison with state-of-the-art on MS-COCO [41]. Our method is the first end-to-end method evaluated on MS-COCO.

## 6. Conclusion

In this paper, we propose the first vision transformer based WSSS framework by exploring the activation mechanism for vision transformers. Specifically, we propose a new activation mechanism GETAM. It shows class-wise attention maps that can better capture the object shape compared to previous approaches. Based on GETAM, we introduce an activation aware label completion module to generate high-quality pseudo labels by adopting foreground saliency information to refine object masks without suppressing non-salient objects in the background. Finally, we present a novel double-backward propagation method to incorporate GETAM into the generation of class activation maps during end-to-end training. Extensive experimental results on both multi-stage and single-stage training show the effectiveness of our method with different vision transformer backbones. The proposed method offers a new perspective for WSSS using vision transformers, and we believe that it can further facilitate the related research areas.



## References

- [1] Jiwoon Ahn, Sunghyun Cho, and Suha Kwak. Weakly supervised learning of instance segmentation with inter-pixel relations. In *IEEE Conference on Computer Vision and Pattern Recognition (CVPR)*, pages 2209–2218, 2019. 7
- [2] Jiwoon Ahn and Suha Kwak. Learning pixel-level semantic affinity with image-level supervision for weakly supervised semantic segmentation. In *IEEE Conference on Computer Vision and Pattern Recognition (CVPR)*, pages 4981–4990, 2018. 1, 2, 3, 5, 7, 8, 14
- [3] Nikita Araslanov and Stefan Roth. Single-stage semantic segmentation from image labels. In *IEEE Conference on Computer Vision and Pattern Recognition (CVPR)*, June 2020. 1, 2, 5, 7, 8, 12
- [4] Sebastian Bach, Alexander Binder, Grégoire Montavon, Frederick Klauschen, Klaus-Robert Müller, and Wojciech Samek. On pixel-wise explanations for non-linear classifier decisions by layer-wise relevance propagation. *PloS one*, 10(7):e0130140, 2015. 2
- [5] Hangbo Bao, Li Dong, and Furu Wei. Beit: Bert pre-training of image transformers, 2021. 2, 6
- [6] Amy Bearman, Olga Russakovsky, Vittorio Ferrari, and Li Fei-Fei. What’s the point: Semantic segmentation with point supervision. In *European Conference on Computer Vision (ECCV)*, pages 549–565, 2016. 1, 2
- [7] Yu-Ting Chang, Qiaosong Wang, Wei-Chih Hung, Robinson Piramuthu, Yi-Hsuan Tsai, and Ming-Hsuan Yang. Mixup-cam: Weakly-supervised semantic segmentation via uncertainty regularization. *arXiv preprint arXiv:2008.01201*, 2020. 2
- [8] Yu-Ting Chang, Qiaosong Wang, Wei-Chih Hung, Robinson Piramuthu, Yi-Hsuan Tsai, and Ming-Hsuan Yang. Weakly-supervised semantic segmentation via sub-category exploration. In *IEEE Conference on Computer Vision and Pattern Recognition (CVPR)*, pages 8991–9000, 2020. 1, 2, 6, 7, 8
- [9] Aditya Chattopadhyay, Anirban Sarkar, Prantik Howlader, and Vineeth N Balasubramanian. Grad-cam++: Generalized gradient-based visual explanations for deep convolutional networks. In *2018 IEEE winter conference on applications of computer vision (WACV)*, pages 839–847. IEEE, 2018. 2, 4
- [10] Hila Chefer, Shir Gur, and Lior Wolf. Generic attention-model explainability for interpreting bi-modal and encoder-decoder transformers, 2021. 2
- [11] Hila Chefer, Shir Gur, and Lior Wolf. Transformer interpretability beyond attention visualization, 2021. 2
- [12] Liyi Chen, Weiwei Wu, Chenchen Fu, Xiao Han, and Yuntao Zhang. Weakly supervised semantic segmentation with boundary exploration. In *European Conference on Computer Vision (ECCV)*, pages 347–362. Springer, 2020. 8
- [13] Liang-Chieh Chen, George Papandreou, Iasonas Kokkinos, Kevin Murphy, and Alan L Yuille. Semantic image segmentation with deep convolutional nets and fully connected crfs. *ArXiv e-prints*, 2014. 1
- [14] Liang-Chieh Chen, George Papandreou, Iasonas Kokkinos, Kevin Murphy, and Alan L Yuille. Deeplab: Semantic image segmentation with deep convolutional nets, atrous convolution, and fully connected crfs. *IEEE Transactions on Pattern Analysis and Machine Intelligence (TPAMI)*, 40(4):834–848, 2017. 1, 7
- [15] Liang-Chieh Chen, George Papandreou, Florian Schroff, and Hartwig Adam. Rethinking atrous convolution for semantic image segmentation. *ArXiv e-prints*, 2017. 1
- [16] Jifeng Dai, Kaiming He, and Jian Sun. Boxesup: Exploiting bounding boxes to supervise convolutional networks for semantic segmentation. In *IEEE International Conference on Computer Vision (ICCV)*, pages 1635–1643, 2015. 1, 2
- [17] Alexey Dosovitskiy, Lucas Beyer, Alexander Kolesnikov, Dirk Weissenborn, Xiaohua Zhai, Thomas Unterthiner, Mostafa Dehghani, Matthias Minderer, Georg Heigold, Sylvain Gelly, Jakob Uszkoreit, and Neil Houlsby. An image is worth 16x16 words: Transformers for image recognition at scale, 2020. 3, 7, 8, 14
- [18] Mark Everingham, Luc Van Gool, Christopher KI Williams, John Winn, and Andrew Zisserman. The pascal visual object classes (voc) challenge. *International Journal of Computer Vision (IJCV)*, 88(2):303–338, 2010. 2, 5, 7, 15
- [19] Junsong Fan, Zhaoxiang Zhang, Chunfeng Song, and Tieniu Tan. Learning integral objects with intra-class discriminator for weakly-supervised semantic segmentation. In *IEEE Conference on Computer Vision and Pattern Recognition (CVPR)*, pages 4283–4292, 2020. 5, 8
- [20] Junsong Fan, Zhaoxiang Zhang, and Tieniu Tan. Employing multi-estimations for weakly-supervised semantic segmentation. In *European Conference on Computer Vision (ECCV)*, pages 332–348, 2020. 8
- [21] Junsong Fan, Zhaoxiang Zhang, Tieniu Tan, Chunfeng Song, and Jun Xiao. Cian: Cross-image affinity net for weakly supervised semantic segmentation. In *AAAI Conference on Artificial Intelligence (AAAI)*, 2020. 1
- [22] Wei Gao, Fang Wan, Xingjia Pan, Zhiliang Peng, Qi Tian, Zhenjun Han, Bolei Zhou, and Qixiang Ye. Ts-cam: Token semantic coupled attention map for weakly supervised object localization, 2021. 2, 3
- [23] Hongyu Guo, Yongyi Mao, and Richong Zhang. Mixup as locally linear out-of-manifold regularization. In *AAAI Conference on Artificial Intelligence (AAAI)*, volume 33, pages 3714–3722, 2019. 1, 2, 6
- [24] Bharath Hariharan, Pablo Arbeláez, Lubomir Bourdev, Subhransu Maji, and Jitendra Malik. Semantic contours from inverse detectors. In *IEEE International Conference on Computer Vision (ICCV)*, pages 991–998. IEEE, 2011. 7
- [25] Seunghoon Hong, Junhyuk Oh, Honglak Lee, and Bohyung Han. Learning transferrable knowledge for semantic segmentation with deep convolutional neural network. In *IEEE Conference on Computer Vision and Pattern Recognition (CVPR)*, pages 3204–3212, 2016. 8
- [26] Qibin Hou, PengTao Jiang, Yunchao Wei, and Ming-Ming Cheng. Self-erasing network for integral object attention. In *Conference on Neural Information Processing Systems (NeurIPS)*, pages 549–559, 2018. 1
- [27] Jie Hu, Li Shen, and Gang Sun. Squeeze-and-excitation networks. In *Proceedings of the IEEE conference on computer vision and pattern recognition*, pages 7132–7141, 2018. 16

- [28] Zilong Huang, Xinggang Wang, Jiasi Wang, Wenyu Liu, and Jingdong Wang. Weakly-supervised semantic segmentation network with deep seeded region growing. In *IEEE Conference on Computer Vision and Pattern Recognition (CVPR)*, pages 7014–7023, 2018. 1, 8
- [29] Peng-Tao Jiang, Qibin Hou, Yang Cao, Ming-Ming Cheng, Yunchao Wei, and Hong-Kai Xiong. Integral object mining via online attention accumulation. In *IEEE International Conference on Computer Vision (ICCV)*, pages 2070–2079, 2019. 5
- [30] Peng-Tao Jiang, Chang-Bin Zhang, Qibin Hou, Ming-Ming Cheng, and Yunchao Wei. Layercam: Exploring hierarchical class activation maps for localization. *IEEE Transactions on Image Processing (TIP)*, 30:5875–5888, 2021. 2, 4
- [31] Beomyoung Kim, Sangeun Han, and Junmo Kim. Discriminative region suppression for weakly-supervised semantic segmentation. In *AAAI Conference on Artificial Intelligence (AAAI)*, pages 1754–1761, 2021. 1, 2, 6
- [32] Alexander Kolesnikov and Christoph H Lampert. Seed, expand and constrain: Three principles for weakly-supervised image segmentation. In *European Conference on Computer Vision (ECCV)*, pages 695–711. Springer, 2016. 8
- [33] Philipp Krähenbühl and Vladlen Koltun. Efficient inference in fully connected crfs with gaussian edge potentials. In *Conference on Neural Information Processing Systems (NeurIPS)*, pages 109–117, 2011. 7, 12, 14
- [34] Jungbeom Lee, Eunji Kim, Sungmin Lee, Jangho Lee, and Sungroh Yoon. Ficklenet: Weakly and semi-supervised semantic image segmentation using stochastic inference. In *IEEE Conference on Computer Vision and Pattern Recognition (CVPR)*, pages 5267–5276, 2019. 5
- [35] Jungbeom Lee, Eunji Kim, and Sungroh Yoon. Anti-adversarially manipulated attributions for weakly and semi-supervised semantic segmentation. In *IEEE Conference on Computer Vision and Pattern Recognition (CVPR)*, pages 4071–4080, 2021. 7
- [36] Jungbeom Lee, Jihun Yi, Chaehun Shin, and Sungroh Yoon. Bbam: Bounding box attribution map for weakly supervised semantic and instance segmentation, 2021. 1, 2
- [37] Seungho Lee, Minhyun Lee, Jongwuk Lee, and Hyunjung Shim. Railroad is not a train: Saliency as pseudo-pixel supervision for weakly supervised semantic segmentation. In *IEEE Conference on Computer Vision and Pattern Recognition (CVPR)*, pages 5495–5505, 2021. 2, 5
- [38] Yi Li, Zhanghui Kuang, Liyang Liu, Yimin Chen, and Wayne Zhang. Pseudo-mask matters in weakly-supervised semantic segmentation. In *Proceedings of the IEEE/CVF International Conference on Computer Vision (ICCV)*, pages 6964–6973, October 2021. 8
- [39] Di Lin, Jifeng Dai, Jiaya Jia, Kaiming He, and Jian Sun. Scribblesup: Scribble-supervised convolutional networks for semantic segmentation. In *IEEE Conference on Computer Vision and Pattern Recognition (CVPR)*, pages 3159–3167, 2016. 1, 2
- [40] Guosheng Lin, Anton Milan, Chunhua Shen, and Ian Reid. Refinenet: Multi-path refinement networks for high-resolution semantic segmentation. In *IEEE Conference on Computer Vision and Pattern Recognition (CVPR)*, pages 1925–1934, 2017. 16
- [41] Tsung-Yi Lin, Michael Maire, Serge Belongie, James Hays, Pietro Perona, Deva Ramanan, Piotr Dollár, and C Lawrence Zitnick. Microsoft coco: Common objects in context. In *European Conference on Computer Vision (ECCV)*, pages 740–755, 2014. 2, 7, 8, 16
- [42] Ze Liu, Yutong Lin, Yue Cao, Han Hu, Yixuan Wei, Zheng Zhang, Stephen Lin, and Baining Guo. Swin transformer: Hierarchical vision transformer using shifted windows, 2021. 2, 6
- [43] Jonathan Long, Evan Shelhamer, and Trevor Darrell. Fully convolutional networks for semantic segmentation. In *IEEE Conference on Computer Vision and Pattern Recognition (CVPR)*, pages 3431–3440, 2015. 1
- [44] Wenfeng Luo and Meng Yang. Learning saliency-free model with generic features for weakly-supervised semantic segmentation. In *AAAI Conference on Artificial Intelligence (AAAI)*, pages 11717–11724, 2020. 8
- [45] Yuxin Mao, Jing Zhang, Zhexiong Wan, Yuchao Dai, Aixuan Li, Yunqiu Lv, Xinyu Tian, Deng-Ping Fan, and Nick Barnes. Transformer transforms salient object detection and camouflaged object detection, 2021. 2, 7
- [46] Youngmin Oh, Beomjun Kim, and Bumsuh Ham. Background-aware pooling and noise-aware loss for weakly-supervised semantic segmentation. In *IEEE Conference on Computer Vision and Pattern Recognition (CVPR)*, pages 6913–6922, 2021. 1, 2
- [47] George Papandreou, Liang-Chieh Chen, Kevin P Murphy, and Alan L Yuille. Weakly-and semi-supervised learning of a deep convolutional network for semantic image segmentation. In *IEEE International Conference on Computer Vision (ICCV)*, pages 1742–1750, 2015. 1, 2, 8
- [48] Pedro O Pinheiro and Ronan Collobert. From image-level to pixel-level labeling with convolutional networks. In *IEEE Conference on Computer Vision and Pattern Recognition (CVPR)*, pages 1713–1721, 2015. 2
- [49] René Ranftl, Alexey Bochkovskiy, and Vladlen Koltun. Vision transformers for dense prediction, 2021. 2, 6, 7, 15
- [50] Anirban Roy and Sinisa Todorovic. Combining bottom-up, top-down, and smoothness cues for weakly supervised image segmentation. In *IEEE Conference on Computer Vision and Pattern Recognition (CVPR)*, pages 3529–3538, 2017. 8
- [51] Ramprasaath R Selvaraju, Michael Cogswell, Abhishek Das, Ramakrishna Vedantam, Devi Parikh, and Dhruv Batra. Grad-cam: Visual explanations from deep networks via gradient-based localization. In *IEEE International Conference on Computer Vision (ICCV)*, pages 618–626, 2017. 3, 4, 13
- [52] Ramprasaath R Selvaraju, Abhishek Das, Ramakrishna Vedantam, Michael Cogswell, Devi Parikh, and Dhruv Batra. Grad-cam: Why did you say that? *arXiv preprint arXiv:1611.07450*, 2016. 2
- [53] Chen Sun, Abhinav Shrivastava, Saurabh Singh, and Abhinav Gupta. Revisiting unreasonable effectiveness of data in deep learning era. In *Proceedings of the IEEE international conference on computer vision*, pages 843–852, 2017. 7

- [54] Guolei Sun, Wenguan Wang, Jifeng Dai, and Luc Van Gool. Mining cross-image semantics for weakly supervised semantic segmentation. *arXiv preprint arXiv:2007.01947*, 2020. 5, 8
- [55] Kunyang Sun, Haoqing Shi, Zhengming Zhang, and Yongming Huang. Ecs-net: Improving weakly supervised semantic segmentation by using connections between class activation maps. In *Proceedings of the IEEE/CVF International Conference on Computer Vision (ICCV)*, pages 7283–7292, October 2021. 4, 8
- [56] Weixuan Sun, Jing Zhang, and Nick Barnes. 3d guided weakly supervised semantic segmentation. In *Asian Conference on Computer Vision (ACCV)*, 2020. 2
- [57] Weixuan Sun, Jing Zhang, and Nick Barnes. Inferring the class conditional response map for weakly supervised semantic segmentation. *arXiv preprint arXiv:2110.14309*, 2021. 1, 4
- [58] Meng Tang, Federico Perazzi, Abdelaziz Djelouah, Ismail Ben Ayed, Christopher Schroers, and Yuri Boykov. On regularized losses for weakly-supervised cnn segmentation. In *European Conference on Computer Vision (ECCV)*, pages 507–522, 2018. 1
- [59] Hugo Touvron, Matthieu Cord, Matthijs Douze, Francisco Massa, Alexandre Sablayrolles, and Hervé Jégou. Training data-efficient image transformers & distillation through attention. In *International Conference on Machine Learning (ICML)*, pages 10347–10357. PMLR, 2021. 7, 8
- [60] Ashish Vaswani, Noam Shazeer, Niki Parmar, Jakob Uszkoreit, Llion Jones, Aidan N Gomez, Lukasz Kaiser, and Illia Polosukhin. Attention is all you need. *arXiv preprint arXiv:1706.03762*, 2017. 1
- [61] Paul Vernaza and Manmohan Chandraker. Learning random-walk label propagation for weakly-supervised semantic segmentation. In *IEEE Conference on Computer Vision and Pattern Recognition (CVPR)*, pages 7158–7166, 2017. 1
- [62] Wenhai Wang, Enze Xie, Xiang Li, Deng-Ping Fan, Kaitao Song, Ding Liang, Tong Lu, Ping Luo, and Ling Shao. Ptv2: Improved baselines with pyramid vision transformer, 2021. 2, 6
- [63] Xinggang Wang, Jiawei Feng, Bin Hu, Qi Ding, Longjin Ran, Xiaoxin Chen, and Wenyu Liu. Weakly-supervised instance segmentation via class-agnostic learning with salient images. In *Proceedings of the IEEE/CVF Conference on Computer Vision and Pattern Recognition*, pages 10225–10235, 2021. 5
- [64] Xiang Wang, Shaodi You, Xi Li, and Huimin Ma. Weakly-supervised semantic segmentation by iteratively mining common object features. In *IEEE Conference on Computer Vision and Pattern Recognition (CVPR)*, pages 1354–1362, 2018. 5, 7, 8
- [65] Yude Wang, Jie Zhang, Meina Kan, Shiguang Shan, and Xilin Chen. Self-supervised equivariant attention mechanism for weakly supervised semantic segmentation. In *IEEE Conference on Computer Vision and Pattern Recognition (CVPR)*, pages 12275–12284, 2020. 1, 2, 4, 6, 8
- [66] Jun Wei, Qin Wang, Zhen Li, Sheng Wang, S Kevin Zhou, and Shuguang Cui. Shallow feature matters for weakly supervised object localization. In *Proceedings of the IEEE/CVF Conference on Computer Vision and Pattern Recognition*, pages 5993–6001, 2021. 4
- [67] Tong Wu, Junshi Huang, Guangyu Gao, Xiaoming Wei, Xiaolin Wei, Xuan Luo, and Chi Harold Liu. Embedded discriminative attention mechanism for weakly supervised semantic segmentation. In *IEEE Conference on Computer Vision and Pattern Recognition (CVPR)*, pages 16765–16774, 2021. 1, 7
- [68] Lian Xu, Wanli Ouyang, Mohammed Bennamoun, Farid Boussaid, Ferdous Sohel, and Dan Xu. Leveraging auxiliary tasks with affinity learning for weakly supervised semantic segmentation. In *Proceedings of the IEEE/CVF International Conference on Computer Vision (ICCV)*, pages 6984–6993, October 2021. 8
- [69] Yazhou Yao, Tao Chen, Guo-Sen Xie, Chuanyi Zhang, Fumin Shen, Qi Wu, Zhenmin Tang, and Jian Zhang. Non-salient region object mining for weakly supervised semantic segmentation. In *IEEE Conference on Computer Vision and Pattern Recognition (CVPR)*, pages 2623–2632, 2021. 1, 5, 8
- [70] Sangdoo Yun, Dongyoon Han, Seong Joon Oh, Sanghyuk Chun, Junsuk Choe, and Youngjoon Yoo. Cutmix: Regularization strategy to train strong classifiers with localizable features. In *IEEE International Conference on Computer Vision (ICCV)*, pages 6023–6032, 2019. 1, 2, 6
- [71] Yu Zeng, Yunzhi Zhuge, Huchuan Lu, and Lihe Zhang. Joint learning of saliency detection and weakly supervised semantic segmentation. In *IEEE International Conference on Computer Vision (ICCV)*, pages 7223–7233, 2019. 2, 8
- [72] Bingfeng Zhang, Jimin Xiao, Yunchao Wei, Mingjie Sun, and Kaizhu Huang. Reliability does matter: An end-to-end weakly supervised semantic segmentation approach. In *AAAI Conference on Artificial Intelligence (AAAI)*, pages 12765–12772, 2020. 1, 2, 6, 7, 8, 12, 15, 16
- [73] Dong Zhang, Hanwang Zhang, Jinhui Tang, Xiansheng Hua, and Qianru Sun. Causal intervention for weakly-supervised semantic segmentation. *arXiv preprint arXiv:2009.12547*, 2020. 8
- [74] Fei Zhang, Chaochen Gu, Chenyue Zhang, and Yuchao Dai. Complementary patch for weakly supervised semantic segmentation. In *Proceedings of the IEEE/CVF International Conference on Computer Vision (ICCV)*, pages 7242–7251, October 2021. 4, 8
- [75] Tianyi Zhang, Guosheng Lin, Weide Liu, Jianfei Cai, and Alex Kot. Splitting vs. merging: Mining object regions with discrepancy and intersection loss for weakly supervised semantic segmentation. In *European Conference on Computer Vision (ECCV)*, 2020. 1, 2, 6
- [76] Zizhao Zhang, Han Zhang, Long Zhao, Ting Chen, and Tomas Pfister. Aggregating nested transformers. In *arXiv preprint arXiv:2105.12723*, 2021. 2
- [77] Hengshuang Zhao, Jianping Shi, Xiaojuan Qi, Xiaogang Wang, and Jiaya Jia. Pyramid scene parsing network. In *IEEE Conference on Computer Vision and Pattern Recognition (CVPR)*, pages 2881–2890, 2017. 1
- [78] Bolei Zhou, Aditya Khosla, Agata Lapedriza, Aude Oliva, and Antonio Torralba. Learning deep features for discrimi-

native localization. In *IEEE Conference on Computer Vision and Pattern Recognition (CVPR)*, pages 2921–2929, 2016. 1, 2, 3, 7, 13

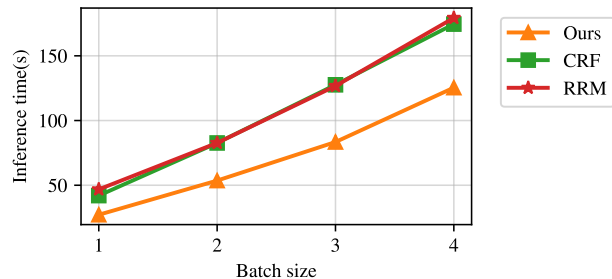


Figure 11. Comparison of inference time of different pseudo label generation methods. The times are computed by the sum of 100 training iterations.

### A. Pseudo Label Generation Computation Time Comparison

In this paper, we propose a fast yet effective pseudo label completion module to generate high-quality pseudo labels. Most existing WSSS methods adopt a multi-step scheme, which requires training multiple networks and has complex interdependencies among steps. Contrarily, in an end-to-end framework, we only have to train a single network in one go. Consequently, in the end-to-end training process, pseudo label generation time is important because we are generating pseudo labels and training the network concurrently, a slow pseudo label generation module would largely influence the overall training speed. In this paper, we propose a fast but effective method to generate high-quality pseudo labels. Except PAMR [3], our generation method is simply based on logical operations without any time consuming modules or networks. To validate that, we present a speed comparison between different pseudo label generation methods.

We test the inference times of pseudo label generation of three methods: our proposed activation aware label completion module, reliable label generation module proposed by RRM [72], and pure CRF [33]. We test on one Nvidia 2080 Ti GPU card, we randomly run for 100 iterations to obtain total inference time with different batch sizes. As shown in Fig. 11, although our pseudo labels have higher quality as presented in Table 1 of main paper, our activation aware label completion module requires much less time compared to competing methods, which can facilitate a more efficient end-to-end training process.

### B. Ablation: High activation Object Mining

In the proposed activation aware label completion module, we propose to mine highly activated regions in the non-salient regions. We argue that since saliency detection models are always trained with foreground objects with center bias, the generated saliency maps on PASCAL VOC



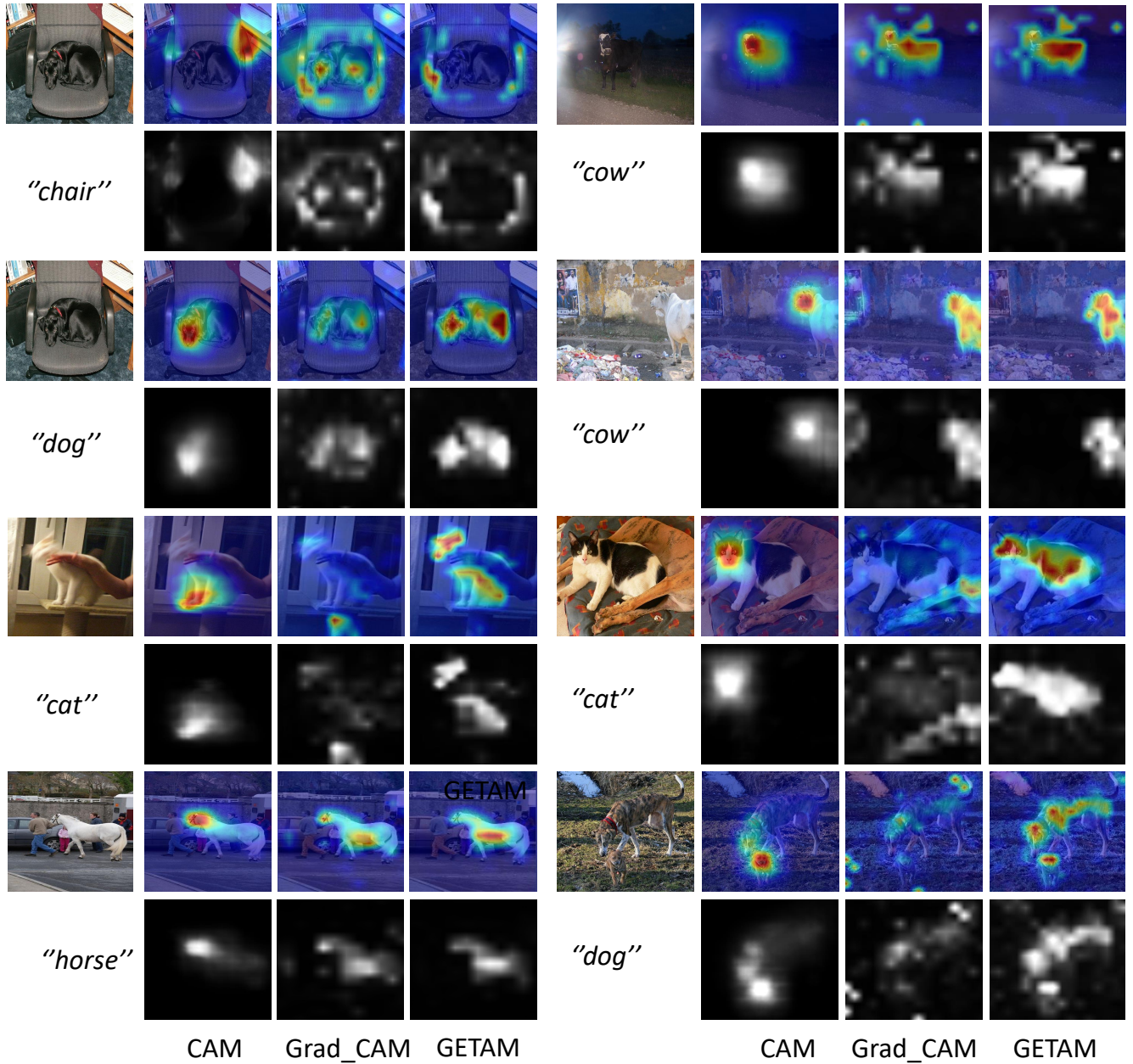


Figure 12. Example images of the proposed GETAM compared to CNN-based CAM [78] and ViT-based Grad-CAM [51]. As discussed in Section 3, naively migrating CAM to vision transformers results in poor results. So we show baseline CAMs obtained from a CNN network, which overly concentrate on discriminative object regions. Second, we migrate Grad-CAM [51] to vision transformer, which can locate objects but may introduce undesired noise. We propose GETAM for vision transformers, which can better capture object shapes and suppress noise than regular CAMs.

may ignore non-salient objects in the background. So after saliency constrained masking, we propose to mine the high activation regions in the background, as these high activation regions are likely to be the erased objects. We set a

threshold  $\alpha$ , if the activation at a pixel of class  $c$  is higher than  $\alpha$  percent of all activation of the same object class, we regard it as highly activated and label it as  $c$ , otherwise as background (0). However, the high activation in the non-

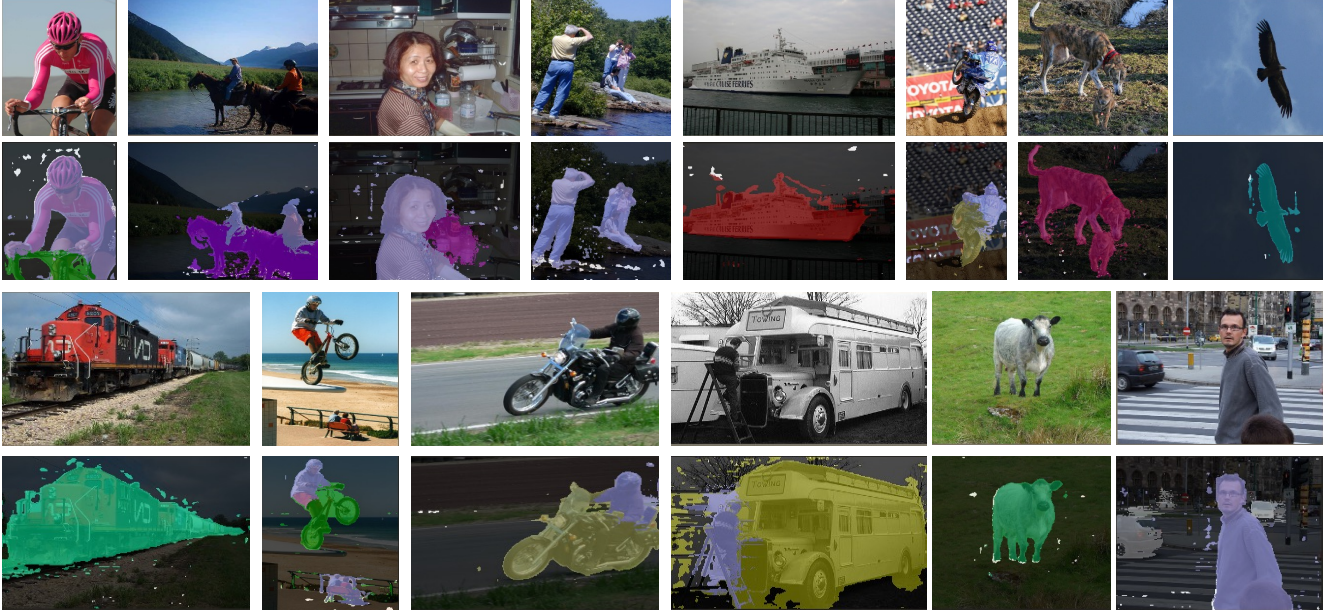


Figure 13. More qualitative results of the pseudo labels generated from the proposed approach. Some tiny noisy regions can be observed in the background areas due to the noise of the saliency maps and activation maps. These tiny regions could be simply erased by a image morphological operation, but due to the robustness of our framework, there is no obvious performance improvement.

| $\alpha$ | 85%  | 90%  | 95%  | 1    |
|----------|------|------|------|------|
| mIoU     | 69.2 | 70.4 | 70.0 | 68.9 |

Table 6. Ablation study for high confidence threshold for non-salient object mining.

salient regions could also be over activated parts of foreground objects or other activation noise. We ablate high confidence  $\alpha$  in Table 6. A small  $\alpha$  means that we only mine a small regions in the background without clear object shape, while a large  $\alpha$  means more complete non-salient object shapes but more noise in the pseudo labels.

Table 6 demonstrates the results of using high confidence threshold from 85% to 100%. When  $\alpha = 100\%$ , we do not perform high activation object mining, *i.e.*, all objects in the non-salient regions are erased, we can observe a performance increment of 2.1% compared to it after utilizing high activation object mining, which validates the effectiveness of the proposed approach. And when  $\alpha = 85\%$ , we can see a performance downgrade, as too many non-salient regions are mined with a lot of noise. We empirically choose  $\alpha = 90\%$  for best performance.

| Method | CRF  | Activation Aware Label Completion |
|--------|------|-----------------------------------|
| mIoU   | 55.1 | 70.4                              |

Table 7. Performance comparison of different pseudo label generation methods: CRF versus our activation aware label completion module, results obtained on ViT-Hybrid [17].

### C. Ablation: Results without Saliency Map

Table 7 shows the effectiveness of our activation aware label completion guided by saliency information. Our proposed GETAM approach with double-backward propagation provides reliable class-wise activation maps during end-to-end training. However, saliency maps are helpful in our case as transformer activation has high object recall but noisy boundaries. During end-to-end training, we follow [2], and add an arbitrary background on activation maps and feed them to a simple CRF [33] to generate pseudo labels, then use these to supervise semantic segmentation. As shown, using a CRF, we can still obtain reasonable results showing reliability of our framework. However, activation aware label completion assisted by saliency maps, yields significantly improved performance, showing the effectiveness of our proposed pseudo label generation module.





Figure 14. Qualitative semantic segmentation results on PASCAL VOC [18] dataset.

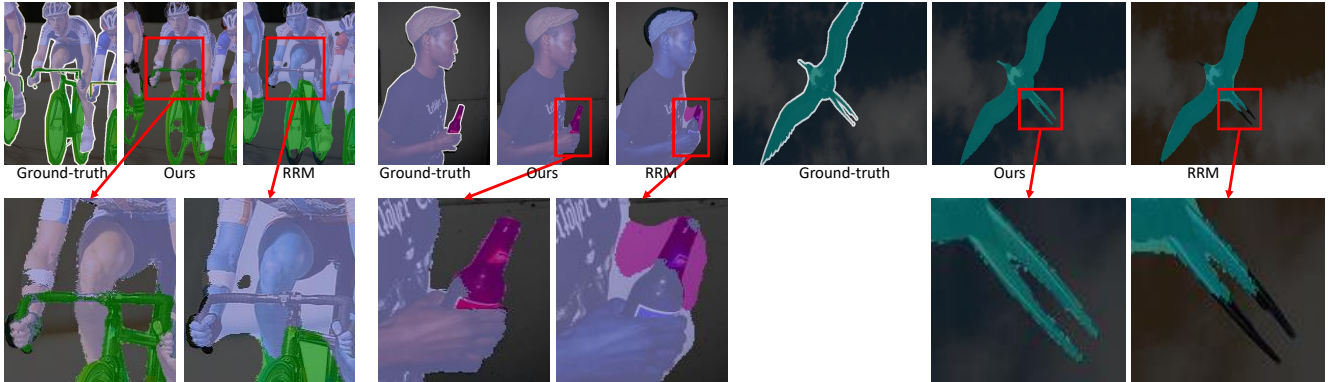


Figure 15. Detail comparison of our segmentation predictions compared to our baseline [72]. Due to the proposed GETAM can capture better object shapes, we can generate high-quality pseudo labels and which lead to segmentation predictions with better fine-grained details.

## D. Segmentation Decoder Structure

In the segmentation branch, we adopt the decoder structure proposed in [49]. We give a detailed introduction of this segmentation decoder.

In this decoder, a set of tokens from multiple levels of transformer blocks are assembled as the image-like features at various resolutions. Since we use the vision transformer backbone with 12 cascaded transformer blocks, we extract

the intermediate output features from the four separated layers following [49]. After obtaining each output features  $O \in \mathbb{R}^{(n+1) \times d}$ , we first map the  $N + 1$  tokens to a set of  $N$  tokens by projecting the CLS token using an MLP to obtain  $O \in \mathbb{R}^{n \times d}$ . Then, since  $n$  is input patch size,  $n = w \times h$ . We reshape the  $O \in \mathbb{R}^{n \times d}$  into an image-like representation by placing each token according to the position of its initial patch in the image  $O \in \mathbb{R}^{h \times w \times d}$ . With these image-like representation maps from four consecutive

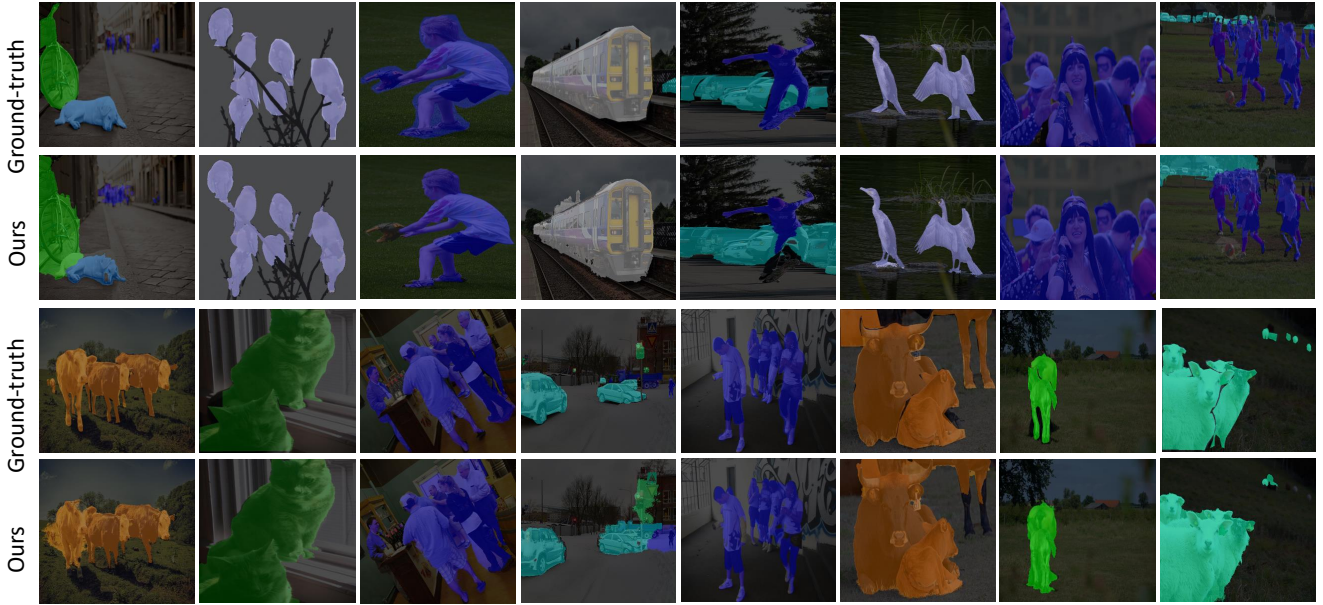


Figure 16. Qualitative semantic segmentation results on COCO dataset [41]. Images from COCO contain multiple objects and more complex scenes, the proposed method can still perform well.

layers of the vision transformer backbone, we apply a RefineNet [40] based decoder structure to combine them. We progressively up-sample the representation by a factor of two in each fusion stage. The output representation size has half the resolution of the input image. Then, we input the output representation into a channel attention block proposed by [27] to obtain final representation output. Finally, we attach a simple semantic segmentation head to make final predictions.

### E. Subsidiary Saliency Loss

During the second stage of our end-to-end training, our loss is defined as  $L = L_{cls} + L_{seg} + L_{sal}$ , where  $L_{cls}$  is multi-label classification loss between the classification predictions and provided class labels. For  $L_{seg}$ , we adopt the semantic segmentation proposed by [72], which consists of cross entropy loss between the semantic segmentation predictions and our pseudo labels, and an energy loss which encourages a better predictions at unlabeled areas (255).

For better object shapes, we present a subsidiary saliency loss during the second stage training. We observe that after pseudo label completion, we can obtain high-quality pseudo labels which can locate objects in both the foreground and background. However, due to the high activation object mining, some noise is generated around foreground objects,

as these regions are likely to be highly activated. Since saliency maps are provided which result in accurate object shapes, we adopt saliency maps as a subsidiary supervision to further refine the boundaries of our semantic segmentation predictions.  $L_{sal}$  is computed as the binary cross entropy loss between the background channels of the predictions and the non-salient regions in saliency maps. Formally, it is defined as:

$$L_{sal} = \alpha * BCE(Seg\_pred[0, :, :], 1 - sal) \quad (6)$$

Where  $1 - sal$  denotes non-salient maps.  $\alpha$  is a tunable weight to control the weight of the  $L_{sal}$  in overall loss. We empirically choose  $\alpha = 0.1$  so we can refine the foreground objects shape without suppressing background objects.